Resources, Conservation & Recycling 186 (2022) 106510

Contents lists available at ScienceDirect

Resources, Conservation & Recycling

journal homepage: www.elsevier.com/locate/resconrec

Plastics and sustainability in the same breath: Machine learning-assisted optimization of coarse-grained models for polyvinyl chloride as a common polymer in the built environment

Hamid Ghasemi, Hessam Yazdani *

Department of Civil and Environmental Engineering, Howard University, 2300 6th St NW #1026, Washington, DC 20059, USA

ARTICLE INFO

Associate Editor: Ming Xu

Keywords:
Sustainability
Optimization
Molecular simulations
Coarse-grained force fields
Machine learning
Polyvinyl chloride

ABSTRACT

The fast-growing construction industry has a vast potential to rise to the plastics challenge by using them in both primary and recycled forms as a sustainable solution to some challenges in the built environment. Improving existing plastics and developing innovative polymers and polymer nanocomposites requires knowledge of interatomic interactions and their influence on macroscopic properties. Coarse-grained (CG) models offer a more computationally efficient alternative to their all-atom counterparts for simulating larger, more representative models of these materials. However, the parameterization and calibration process of CG force fields (CG-FFs) commonly entails solving a nonconvex optimization problem involving numerous local minima, rendering traditional optimization techniques impractical and iterations based on educated guesses inefficient. Here, we develop an approach to efficiently parameterize a CG-FF by coupling a metaheuristic algorithm as the calibrator (optimizer) with support vector regression-based surrogate models trained using molecular dynamics data. The merit of the approach is demonstrated by parameterizing a CG-FF potential for polyvinyl chloride (PVC) as a representative general-purpose plastic with many applications in the construction industry. The generalizability of the CG-FF to large PVC models in both pristine and carbon nanotube-filled composite forms is demonstrated. The CG-FF also accurately reproduces glass transition temperature and thermal conductivity as unseen properties of PVC.

1. Introduction

The expanding construction industry has a vast potential to rise to the plastics challenge and contribute to stimulating a more resource-efficient, circular economy. For one thing, discarded plastics can be repurposed for construction applications, saving space in landfills and reducing construction costs, among other benefits (Kazemi et al., 2021; Fini et al., 2021; Zakertabrizi et al., 2021; Kazemi and Fini, 2022). And for another, characteristics such as strength, lightness, durability, impermeability, affordability, and moldability make plastics a competitive engineering solution to some challenges in the built environment. Geosynthetics, for instance, are one of the salient examples of plastics/polymers in the built environment that offer multiple functions such as reinforcing roads, stabilizing steep soil embankments and bridge abutments, controlling coastal erosion, and lining landfills, canals, water storage facilities, and wastewater treatment lagoons, all at considerably reduced levels of CO_2 emission, soil acidification, and eutrophication compared with conventional construction materials and techniques (Puppala et al., 2020; Shukla, 2021).

Improving the properties and durability of existing polymers and polymer nanocomposites (PNCs) and developing novel polymeric products, especially for construction purposes, can further reduce the environmental impact and embodied carbon of these materials and promote sustainability. However, the traditional development cycle of polymers and PNCs typically involves educated guesses or Edisonian techniques that often yield incremental advances but with limited efficiency. Computational approaches to materials design such as numerical simulations and predictive modeling offer the potential to 'short-circuit' this development cycle by making it possible to investigate scenarios that would otherwise be difficult/impossible to investigate in the laboratory. These approaches also offer insight into the phenomena and mechanisms governing the behavior of materials, reducing the time and resources necessary to engineer innovative, lightweight, high-performance, multifunctional polymers and PNCs. These approaches,

* Corresponding author.
E-mail address: hessam.yazdani@howard.edu (H. Yazdani).

https://doi.org/10.1016/j.resconrec.2022.106510
Received 31 March 2022; Received in revised form 10 June 2022; Accepted 1 July 2022
Available online 20 July 2022

however, are demanding, emphasizing the need to develop more computationally benign models and techniques.

In computational and statistical mechanics, coarse-graining involves constructing and parameterizing (calibrating) a sufficiently accurate representation of an atomistic/molecular system. The reduced degrees of freedom and number of highly fluctuating particles (e.g. light atoms such as hydrogen) in coarse-grained (CG) models results in a smoother energy landscape that, depending on energy oscillations, often allows for analyzing structures and processes that transcend length and time-scales accessible to all-atom molecular dynamics (AA-MD). Several coarse-graining methods exist that offer different degrees of structural and statistical equivalence to the reference system, depending on the system characteristics and the basis used for parameterization. These methods can broadly be categorized into two main themes: top-down and bottom-up. The top-down theme involves parameterizing force fields using experimental macroscopic data, whereas in the bottom-up theme data such as forces or structural probability distributions from more detailed simulations are employed as the basis for the force field parameterization (Sun et al., 2021). Examples of bottom-up methods include the iterative Boltzmann inversion method (Müller-Plathe, 2002; Rudzinski and Noid, 2015), the Martini force field (Marrink et al., 2007), and the energy-conservation approach (Español et al., 2016). These methods differ in convergence rate (e.g. the iterative Boltzmann inversion method is often slow (Jain et al., 2006)), the chemical specificity they represent, and the type and level of details they provide (e.g. the Martini force field does not provide structural details for a specific system (Arash et al., 2015)), among other factors. The optimal choice of coarse-graining method will depend on the material in hand, quantities of interest (i.e. properties), and which side of the model simplicity-physical realism (i.e. computational efficiency-accuracy) trade-off one would wish to stand.

AA data are a common basis in bottom-up CG force field (CG-FF) parameterization where several neighboring particles (e.g. functional groups or molecular subunits) are lumped into extended interaction clusters known as beads or blobs, followed by defining the bonded (e.g. via springs) and nonbonded interactions among the beads by force field parameterization. Such reduced degrees of freedom associated with coarse-graining introduce uncertainties into the simulation results. These uncertainties are commonly addressed by performing calibration and validation tests over select parameters to match CG and AA data (e.g. force-matching (Liwo and Czaplewski, 2020)). The process is formulated as a minimization (optimization) problem with the objective (cost) function defined as the difference in the predictions made for quantities of interest by the CG and AA models (Oden et al., 2015). For materials like polymers that feature a wide range of compositions, phenomena, and interactions occurring across several scales of time, length, complexity, and uncertainty, such optimization problems would be highly nonlinear. Solving such problems would entail extensive sampling to effectively explore and exploit the force field parameters space, rendering traditional optimization methods impractical and iterations based on educated guesses inefficient (Christensen et al., 2021). Therefore, it appears to be reasonable to target a limited number of quantities of interest (e.g. elastic modulus) and optimize the CG-FF parameters for them to reduce the complexity and computational costs of the problem. Some shortcomings, however, will inevitably ensue. For example, by targeting specific quantities of interest, one may need to compromise on the accuracy of predictions made by the CG-MD model for less important polymer features (e.g. melting temperature (Oden et al., 2013)). Nevertheless, such an approach would reduce the computational burden of the problem to the level that can be managed using machine learning-assisted metaheuristic optimization.

A known characteristic of structure-based CG simulations of soft matter is that the dynamics involved are artificially accelerated (Eslami et al., 2019). In case the experimental/fully-atomistic dataset is relatively small, this characteristic implies that CG dynamical features mainly characterized by structural attributes such as angle and bond distributions of connected beads in polymer chains cannot readily be compared with the dataset in absolute terms (Eslami and Müller-Plathe, 2013). This study hypothesizes that such small datasets can be used to develop scalable and generalizable CG models that will reproduce specific quantities of interest (here, mechanical properties and density) of the polymer while capturing the chain dynamics and other properties only to a reasonable extent. The hypothesis is tested by parameterizing and calibrating a CG-FF given a limited dataset. The approach involves coupling the particle swarm optimization (PSO) algorithm as the calibrator (optimizer) with support vector regression (SVR) surrogate models as the predictors. The efficiency of the approach is demonstrated by applying it to polyvinyl chloride (PVC) as a representative general-purpose plastic for which, to the best of our knowledge, no CG-FF has been reported. The scalability of the CG-FF to larger PVC models and its generalizability to PVC nanocomposites are also demonstrated.

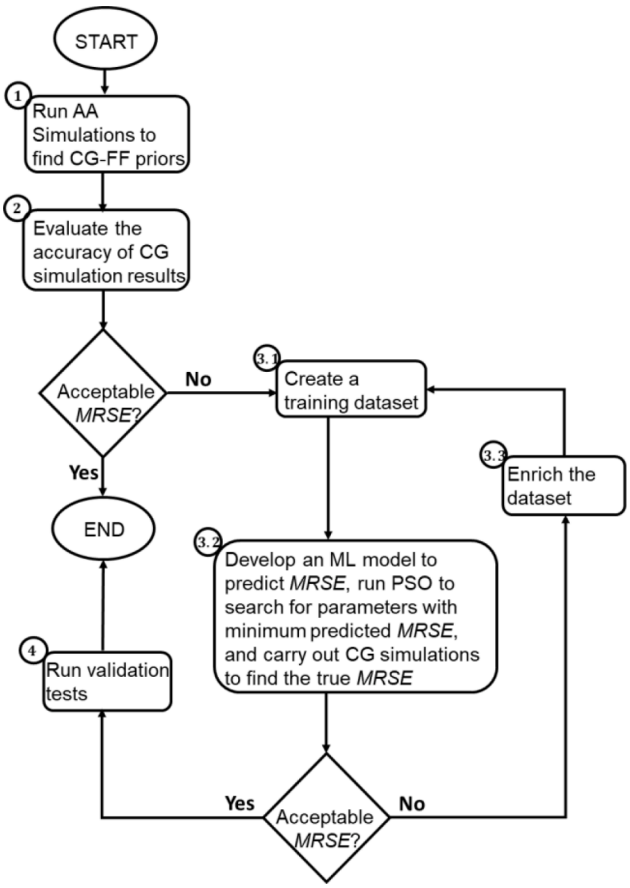

Fig. 1. Flowchart of the approach devised and used in this study to develop a CG model. A description of the task that each symbol entails is provided in the text with the heading "Step (insert the number attached to the symbol)".

2. Methodology

2.1. Quantifying and calibrating CG priors

Finding the CG priors and the calibration process consisted of four steps, as described below and summarized in Fig. 1.

Step 1- Find CG priors using AA-MD: This step involved finding a set of CG-FF parameters by which each energy component (as introduced later in this section) of the CG model would be independently equivalent to the energy of its AA model. To this end, PVC monomers (C_2H_2Cl) were represented by beads in the CG model, and their interactions were described using the consistent-valence force field (Hagler et al., 1979)

Table 1
Energy formulations and CG input parameters.

AA representation	CG representation	Energy component	CG CVFF expression	CG parameters
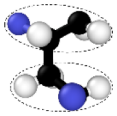		Bond energy	$E_b = K_r(r - r_0)^2$	K_r, r_0
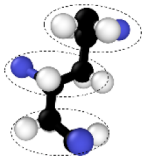		Angle energy	$E_\theta = K_\theta(\theta - \theta_0)^2$	K_θ, θ_0
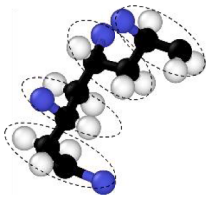	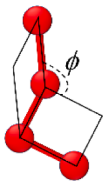	Torsion energy	$E_\Phi = K_\Phi(1 - \cos\Phi)$	K_Φ
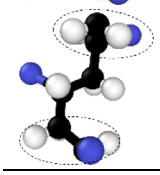	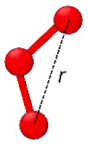	Nonbonded energy	$E_{vdW} = 4\varepsilon[(\sigma/r)^{12} - (\sigma/r)^6]$	ε, σ

(CVFF) with the seven parameters shown in Table 1. CVFF was also used for the AA simulations. The FF has five energy components, including bond stretch, angle, torsion, van der Waals (vdW), and Coulombic and has successfully been used in both AA and CG simulations to predict a wide range of properties for polymer and polymer composites (Lange et al., 2016). Here, the first four energy components were considered for CG simulations, and Coulombic interactions were excluded, given the electrical neutrality of the beads.

A harmonic expression was used to describe the bond stretch interaction (bond energy) between every pair of bonded beads (see Table 1 for the formulation). To quantify (i.e. finding the priors of) the bonding parameters (i.e. r_0 and K_r), an AA model made of one chain with 1,000 monomers was relaxed at the temperature of 300 K under the canonical ensemble (NVT) for 2 ns, followed by 2 ns relaxation at no pressure under isothermal-isobaric (NPT) ensemble. Simulations were repeated three times with different seed numbers to account for the randomness in the initial velocity distribution of atoms. In the last 1 ns of the NPT relaxation stage, eight monomers (two groups of four successive monomers) were randomly selected, and the most frequent distance (r) between their centers of mass (COMs) was taken for r_0 in the CG model. Next, the bond energy of each pair of neighboring monomers was divided by $(r - r_0)^2$ of each pair of beads, and the most frequent resulting value was assigned to K_r.

The angle energy was also expressed as a harmonic formulation. Similarly, eight monomers in each simulation (two groups of four successive monomers) were randomly picked to find the equilibrium angle, θ_0, between every three consecutive monomers. Then, the angle energy was divided by $(\theta - \theta_0)^2$, and the most frequent value was given to K_θ.

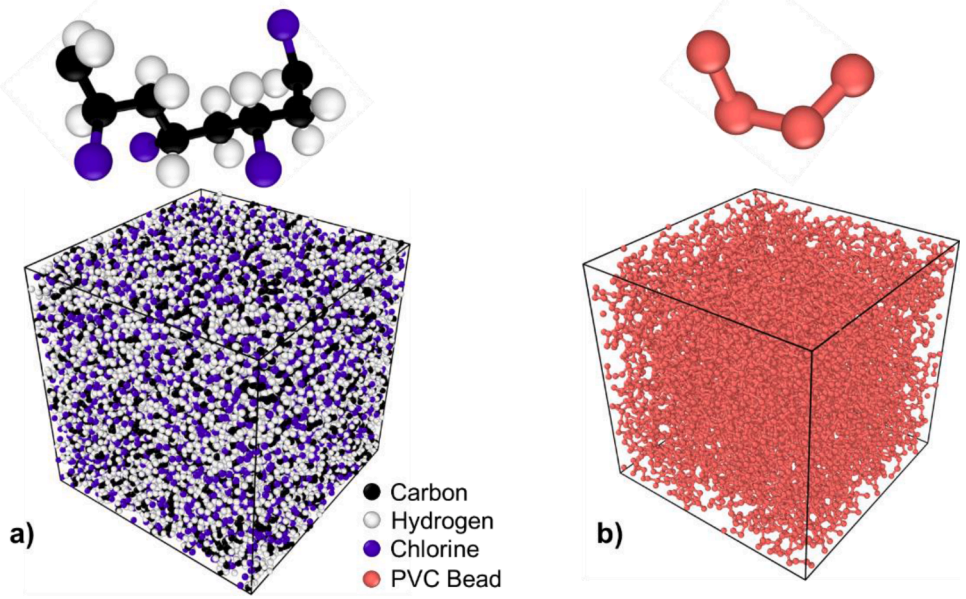

Fig. 2. a) The AA model containing seven chains, each having 1,000 PVC monomers, and b) its equivalent CG model.

The torsion (dihedral) angle is defined as the angle between two intersecting planes, each formed by three beads. The planes share the two middle beads. Here, eight monomers (two groups of four successive monomers) were randomly selected to calculate the torsion angle, which was later divided by (1 - cosΦ) to find the torsion stiffness (K_Φ).

The nonbonded priors (ε ['dispersion energy'] and σ ['size of the particle']) were represented by the most frequent inter-monomer energy and distance observed among nonbonded monomers.

Step 2- Evaluate accuracy of the priors: The accuracy of the priors obtained in Step 1 was evaluated by comparing the density and tensile stress-strain response of a CG model defined by them and those of the reference AA model. For comparison, the CG model comprised seven chains of 1,000 PVC beads each (Fig. 2). The chains were generated using the self-avoiding random walk technique (Hossain et al., 2010). Each chain started from a random site and then grew in length by moving randomly from a current site to one of its nearest neighbors according to a uniform probability density function until a certain number of sites equal to the degree of polymerization (i.e. 1,000 beads) were visited. Every two neighboring beads were linked with a chemical bond, and the priors and potential functions described and quantified in Step 1 were assigned to the model. The stress-strain responses were established by uniaxially stretching the models. All simulations were performed with LAMMPS (Plimpton, 1995) and visualized with OVITO (Stukowski, 2009). A time step of 0.5 fs and a deformation velocity of 10^{-4} (Å/fs) were used in all (both AA and CG) simulations. In all CG-MD simulations, the cutoff was selected to be 12 Å. Stress values were recorded at 10 strain values from 0.5–5% with 0.5% increments in both CG and AA simulations. The error was represented by the root-mean-square values of the deviation of the stress value given by the CG-MD simulation from that given by the AA-MD simulation at a particular strain normalized with respect to the stress value given by the AA-MD simulation, as:

$$\boldsymbol{RMSE} = \sqrt{1 \Big/ \boldsymbol{n} \sum_{i=1}^{10} \left[\frac{(\boldsymbol{\sigma_{CG}})_i - - (\boldsymbol{\sigma_{AA}})_i}{(\boldsymbol{\sigma_{AA}})_i} \right]^2} \quad (1)$$

where $(\sigma_{CG})_I$ and $(\sigma_{AA})_i$ represent the stresses computed at the i-th strain value in the CG-MD and AA-MD simulations, respectively.

Step 3- Develop a surrogate model to predict RMSE: As shown later, an independent evaluation of energy components (potential functions) in Step 1 typically results in values for the priors that fail to collectively reproduce the response of the AA model, leading to large errors (i.e. *RMSE* values). Therefore, the priors should be calibrated to reduce the error. Such calibration, however, would entail adjusting the values iteratively and evaluating *RMSE* in each iteration until an acceptable *RMSE* value is achieved. Since the number of iterations is problem-specific and unknown, the computational expense of such an approach could be prohibitive. As previously alluded, machine learning predictive models (surrogate or metamodels models) can significantly alleviate this computational cost and accelerate the calibration process. The following sub-steps were taken to develop surrogate models with MATLAB R2019b.

3-1- Create a training dataset: The priors and their corresponding *RMSE* values were treated as the reference observation. A set of 42 additional observations was made as follows to construct a dataset: for each observation, all the priors were held constant at their reference value except one prior that was either increased or decreased by 10%, 30%, and 50%, yielding a total of 42 additional observations (7 priors × 3 ±%). Note that the upper bound for the equilibrium angle parameters, θ_0, was set at its maximum physically possible value of 180° (i.e. a maximum of 40% increase).

3-2- Develop surrogate models to predict RMSE and density: Since the dataset in this study was also relatively small, support vector regression (SVR) was used to predict *RMSE* (more information to follow). For each SVR model, hyperparameters were tuned to achieve the lowest prediction error (mean square error). Also, one-leave-out cross-validation (LOO-XV) was used to prevent overfitting. This means that with a dataset of size *N*, the predictor was trained *N* separate times on all the data except for one data point, a prediction was made for that point, and the average error was finally computed and used to evaluate the model. Another SVR model was developed following the same approach to predict density.

3-3- Expand the dataset and improve the predictive models: Following training and tuning hyperparameters, the SVR models were coupled with an optimization algorithm, described in the next section, to strategically take samples from a wide range of values (±50% of the reference value, except the equilibrium angle which was bounded between -50% and +40% of its prior) for the CG-FF parameters and iteratively calibrate the priors. The best solution offered by the optimization algorithm at the end of each iteration (i.e. the combination associated with the minimum predicted *RMSE* value) was used to simulate a CG model comprising seven 1,000-monomer chains (7,000 monomers in total) to compute the solution's true *RMSE* value. The combination and its true *RMSE* value were then added to the training dataset to improve the accuracy of the SVR models. This process continued until a combination (calibrated priors) with a desirable *RMSE* level was found.

Step 4- Validate generalizability of the calibrated priors: The generalizability of the calibrated priors to larger models and composite systems was validated by demonstrating their capability to reproduce the tensile response of AA models composed of 20 and 40 1,000-monomer chains (20,000 and 40,000 monomers in total) in both pristine form and composite form reinforced with one (5,5) carbon nanotube (CNT) with an aspect ratio of 157 (CNT concentration: 2.5 wt.%).

2.2. Optimization Problem and Approach

2.2.1. Optimization problem

The optimization problem can be expressed as:

$$\begin{aligned} &\text{Find :} && K_r,\ r_0,\ K_\theta,\ \theta_0,\ K_\varphi,\ \varepsilon,\ \sigma \\ &\text{Minimize :} && RMSE \\ &\text{subject to :} && \Theta_{\min} \le\ \Theta \le \Theta_{\max} \end{aligned} \quad (2)$$

where Θis a vector representing the values of the seven parameters to be quantified by the optimization algorithm, and$\Theta_{\min}$and $\Theta_{\max}$include the lower and upper limits of the values, respectively.

2.2.2. Particle swarm optimization

Metaheuristics are problem-independent and versatile techniques that have proven efficient in solving various optimization problems. Compared with now-traditional gradient-based optimization techniques, the stochastic mechanism inherent in metaheuristics allows them to effectively explore and exploit a vast search space enclosed by highly nonlinear and discontinuous constraints without requiring gradient information and explicit formulations for the objective function and constraints (Khatibinia and Yazdani, 2018; Shayesteh Bilondi et al., 2018). A class of metaheuristics, swarm-based metaheuristic techniques iteratively converge to the optimum solution(s) by comparing the solutions offered by the swarm in each iteration. Since the optimization process could involve a large swarm of agents and numerous iterations, it could be computationally intractable if the solutions were to be MD-simulated for objective function evaluations. One approach that has proven effective at considerably alleviating the computational cost associated with evaluating the objective function is to use machine learning predictive (surrogate) models. Such models approximate the objective function and constraints with an accuracy that depends on the nature of the problem and the data used to train the models, hence considerably accelerating the optimization process (Yazdani et al., 2017b; Gharehbaghi et al., 2019).

Particle swarm optimization (PSO) is an optimization technique inspired by swarm intelligence, which is the collective behavior of a

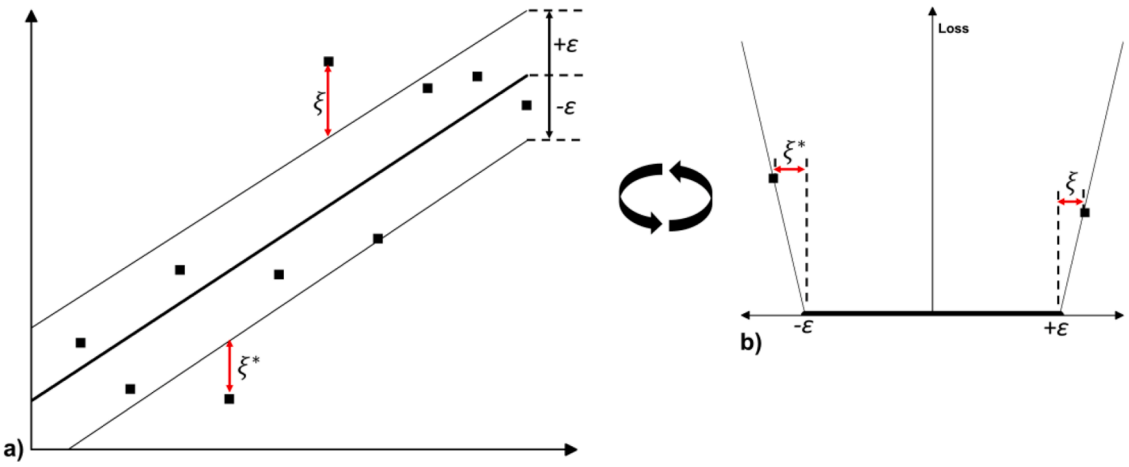

Fig. 3. a) a linear SVM regression with b) an ε-insensitive loss function and slack variables. SVM hyperparameters are iteratively tuned to get the lowest prediction errors (Vapnik, 2000).

swarm capable of accomplishing complex tasks in dynamic and varied environments without any central coordination, external guidance, or control (Kennedy and Eberhart, 1995). PSO imitates the choreography and sociocognitive behavior of birds in a flock (swarm). The birds are dubbed 'agents' or 'particles.' Each agent represents a possible solution in the search space. Agents quasi-randomly fly around and iteratively move toward the optimum solution (food). They achieve this by keeping an eye on others to follow the agent closest to the optimum solution (g_{best}) while keeping track of their own best solutions found so far (p_{best}). The i-th agent in the l-th iteration is associated with a position vector $\mathbf{X}_i^l$ and a velocity vector $\mathbf{V}_i^l$ denoted as

$$\begin{aligned}\mathbf{X}_i^l &= \left\{ x_{i,1}^l, x_{i,2}^l, \ldots, x_{i,p}^l \right\} \\ \mathbf{V}_i^l &= \left\{ v_{i,1}^l, v_{i,2}^l, \ldots, v_{i,p}^l \right\}\end{aligned} \tag{3}$$

where p is the dimension of the solution space (here 7, see Table 1). As an agent navigates the solution space, its position is updated as:

$$\mathbf{V}_i^{l+1} = \omega^l \mathbf{V}_i^l + c_1 r_1 \left(\boldsymbol{pbest}_i^l - \boldsymbol{X}_i^l \right) + c_2 r_2 \left(\boldsymbol{gbest}^l - \boldsymbol{X}_i^l \right) \tag{4}$$

$$\boldsymbol{X}_i^{l+1} = \boldsymbol{X}_i^l + \boldsymbol{V}_i^{l+1} \tag{5}$$

where r_1 and r_2 are two uniform random numbers between (0, 1); c_1 and c_2 are the cognitive- and social-scaling parameters, respectively; and ω^l is the inertia weight that controls the influence of the previous velocity and is defined in the l-th iteration as (Shi and Eberhart, 1998):

$$\omega = \omega_{\max} - \frac{\omega_{\max} - \omega_{\min}}{l_{\max}} \, l \tag{6}$$

where $\omega_{\max}$and$\omega_{\min}$are the maximum and minimum values of ω, respectively; and l_{max} is the maximum number of iterations. The following values were used in this study for the parameters described above: $c_1 = 2.5$, $c_2 = 2.5$, $\omega_{\max} = 0.9$, and $\omega_{\min} = 0.01$. The population size (N) and the maximum number of iterations (l_{max}) were set to 50 and 200, respectively. These values were selected by trial and error and per our experience and general recommendations in the literature (Shayesteh Bilondi et al., 2018). These values are also consistent with those used in a recent study on developing an interatomic potential for glassy silica using PSO (Christensen et al., 2021).

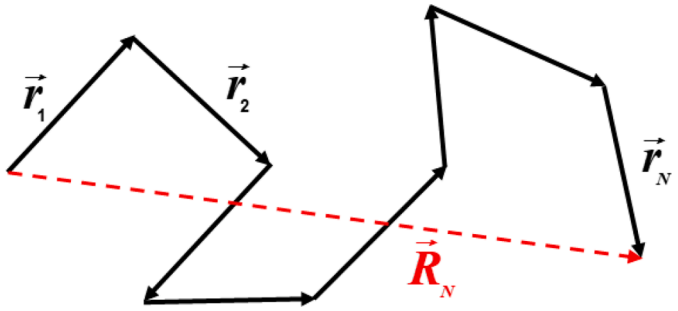

Fig. 4. End-to-end distance in a schematic chain of polymer.

2.3. Support vector regression

Support vector regression (SVR; the regression equivalent of support vector machines/classifiers) was used to develop the surrogate models. SVR has the advantages of generalizability and ease of use. SVR aims to construct a hyperplane that is close to as many of the data points as possible. Therefore, it can achieve good generalizability by minimizing the prediction error as tuning its hyperparameters is obtained by cross-validation (Chen et al., 2018). The structural risk minimization (SRM) principle in SVR makes it less prone to overfitting than convolutional neural networks that use the empirical risk minimization (ERM) principle. In contrast to ERM, which shrinks the prediction error on the training data, SRM reduces an upper bound on the expected prediction risk to make SVR generalizable. To both reduce the prediction error and enhance the generalizability of an SVR model, SVR can be trained based on the ε-insensitive loss function (Mozer et al., 1997). The ε-insensitive loss function uses margins in regression such that if the error is smaller than ε, the prediction error will be assumed to be zero. Therefore, for a linear regression function $f(x)$:

$$f(x) = \langle w \, . \, x \rangle + b \tag{7}$$

where w is the weight error, x is the input vector, and b is the bias of the regression function. The SRM principle can be formulated by minimizing the empirical risk R_{emp} (w, b) defined as:

$$\text{Remp}\ (\text{w},\ \text{b}) = 1 \Big/ \text{n} \sum_{i=1}^{n} L_\varepsilon(y_i,\ f(x)) \tag{8}$$

where L_ε is the loss function, and y represents the true output. Then, the ε-insensitive loss function finds the following form:

$$L\varepsilon\ (yi,\ f(x)) = \left\{ \begin{array}{c} 0,\ if\ |y_i - f(x)| \le \varepsilon \\ |y_i - f(x)| - \ \varepsilon,\ otherwise \end{array} \right\} \tag{9}$$

Finding w and b to reduce the ERM with respect to the ε-insensitive loss function is a convex optimization problem that minimizes the margin and two non-negative slack variables, ξ and ξ^*, as:

$$\text{Minimize}: \left[\frac{1}{2}\|w\|^2 + C\sum_{i=1}^{m}(\xi_i + \xi_i^*)\right]$$

$$\text{Subject to}: \begin{cases} y_i - w.x_i - b \le \varepsilon + \xi_i \\ w.x_i + b - y_i \le \varepsilon + \xi_i \\ \xi_i, \xi_i^* \ge 0 \end{cases} \quad (10)$$

where $C > 0$ is known as 'penalty' or 'regularization' or 'box constraint' and governs the trade-off between the model complexity and the influence of deviations larger than ε on the regressor (Smola and Schölkopf, 2004). A representation of the linear SVM regression is shown in Fig. 3. For nonlinear SVM regressions, the line shown in Fig. 3a is replaced by a hyperplane, and x in Eq. (7) is replaced by a function called 'kernel function' denoted by $\varphi(x)$. Polynomial and gaussian (also known as the radial basis) kernels are popular kernel functions widely used in the materials engineering literature (Lu et al., 2013; Mannodi-Kanakkithodi et al., 2016). As shown in Fig. 3, hyperparameters of an SVM regressor, penalty, the kernel function, and ε should be optimized iteratively such that the regressor finds the minimum prediction error. In this study, the quadratic kernel function and a C value of 567.7 were used, and the hyperparameters of the SVM regressor were tuned such that the mean square error (MSE) of *RMSE* predictions would be minimized.

2.4. Evaluation of accuracy of CG parameters

The CG-FF was examined for its accuracy in reproducing glass transition temperature, thermal conductivity, and end-to-end distance of polymer chains as unseen properties beyond the properties that the CG-FF was optimized against (i.e. mechanical and density).

2.4.1. Mechanical properties

The uniaxial strain-stress behavior of PVC and CNT-filled PVC composites up to 5% of strain was used to represent mechanical properties.

2.4.2. Glass transition temperature

The glass transition temperature (T_g) of a polymer is the temperature associated with a distinct transition of (amorphous regions in) the polymer from a hard, glassy state to a soft, rubbery state where polymer chains obtain full segmental mobility. T_g corresponds to the point of maximum curvature in the temperature-volumetric strain curve. To calculate the T_g of PVC, its structure was first relaxed at an initial temperature of 500 K, which is higher than the 341–373 K range reported for the T_g of PVC (Cui et al., 2017). While maintaining the pressure components at zero, the temperature was then decreased to 100 K at a cooling rate of 1 K/ps, and volume change was recorded and plotted to find T_g.

2.4.3. Thermal conductivity

Four main methods can be used to calculate the thermal conductivity of materials using MD simulations. These include equilibrium molecular dynamics (EMD - (Bagri et al., 2011)), approach-to-equilibrium molecular dynamics (AEMD - (Lampin et al., 2013)), nonequilibrium molecular dynamics (NEMD - (Razzaghi et al., 2021)), and reverse nonequilibrium molecular dynamics (RNEMD - (Müller-Plathe and Bordat, 2004)). Among these four, EMD and RNEMD are more popular and have widely been used to calculate the thermal conductivity of polymers (Eslami et al., 2011, p. 6; Lussetti et al., 2007, p. 6; Vasilev et al., 2020). In this study, EMD and RNEMD were used to calculate the thermal conductivity of AA and CG models.

- EMD

The EMD approach uses Green-Kubo formulas (Kubo, 1957) to relate the ensemble average of the autocorrelation of the heat flux (**J**) to thermal conductivity κ, as:

$$\kappa = \frac{V}{k_B T^2}\int_0^\infty J_x(0)J_x(t)dt = \frac{V}{3k_B T^2}\int_0^\infty J(0)J(t)td \quad (11)$$

where V is volume, T is temperature, and k_B is the Boltzmann constant. In this study, to calculate the heat flux autocorrelation function in MD simulations, the trajectories of atoms in the AA model and beads in the CG model were updated with the microcanonical ensemble (NVE) for 2.5 ns, and the thermal conductivity of PVC was averaged in the three principal directions.

RNEMD

The RNEMD approach imposes heat flux by periodically exchanging kinetic energy between two atoms in two different regions and calculates the induced temperature gradient as system response. RNEMD is based on the Muller-Plathe algorithm (Müller-Plathe, 1997), where the periodic simulation box is divided into N bins (N is an even number) along the dimension of interest (e.g. x), followed by swapping the kinetic energy every user-defined number of steps between N_{swap} atoms with the highest kinetic energy in the 1st bin and N_{swap} atoms with the lowest kinetic energy in the $(N/2+1)^{th}$ bin. This process eventually establishes two symmetric temperature gradients dT/dx on both sides of the simulation box that can be plugged into Fourier's law (law of heat conduction) to calculate thermal conductivity:

$$Q = -\kappa A dT/dx \quad (12)$$

where Q is the swapped kinetic energy, A is the cross-sectional area perpendicular to the x dimension, and T is temperature. In this study, $N = 40$ and $N_{swap} = 10$ were used, and the swapping was performed every 1,000 time steps.

Table 2
Prior values obtained for the force field parameters.

Force field parameters (priors)	Value
r_0 (Å)	3.6
K_r (kcal/mol/Å^2)	10.0
θ_0 (°)	127.0
K_θ (kcal/mol/rad^2)	5.0
K_Φ (kcal/mol)	5.8
ε (kcal/mol)	2.2
σ (Å)	5.5

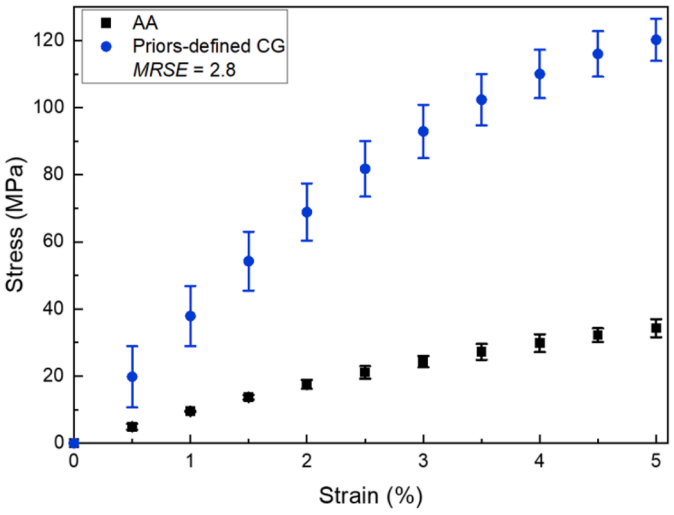

Fig. 5. Comparison of strain-stress response of the AA model with that of the 7,000-bead CG model defined by the CG-FF values. The error bars represent one standard deviation from the mean values of three simulations with different seed numbers.

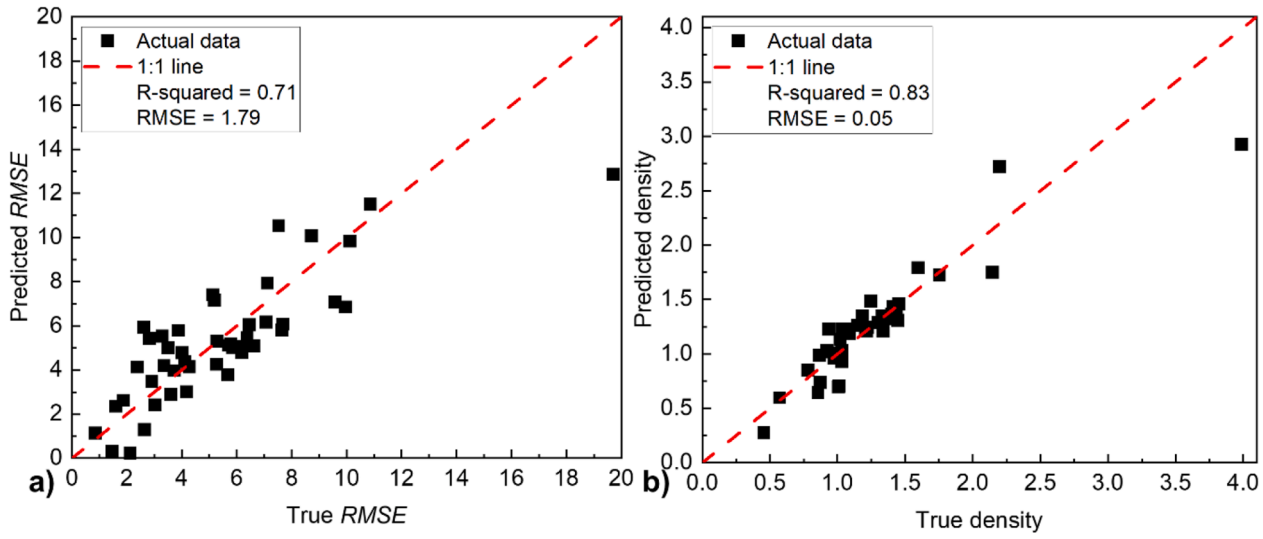

Fig. 6. Performance of SVR models (entire data: [reference + 42 ±% observations] × three iterations) in predicting a) *RMSE* and b) density.

2.4.4. End-to-end distance

In the physical chemistry of polymers, the vector that starts from one end of a polymer chain (first monomer in the chain) and points to the other end of the chain (last monomer in the chain) is called the end-to-end vector. The end-to-end distance of a polymer chain is defined as the magnitude of the end-to-end vector. The end-to-end distance is used to evaluate whether the developed CG-MD model retained the structural features of the corresponding AA-MD model.

Here, the end-to-end distances of the AA-MD model and CG-MD model made of 7,000 monomers (7 chains of 1,000 monomers) were calculated and compared against each other.

3. Results and discussion

3.1. Priors

The priors obtained for the CG-FF parameters are shown in Table 2. These values were used to define the interactions in the CG model comprising seven chains of 1,000 beads each. The simulation yielded a density of 1.18 g/cm^3, which agrees well with that of 1.22 g/cm^3 computed for the AA model.

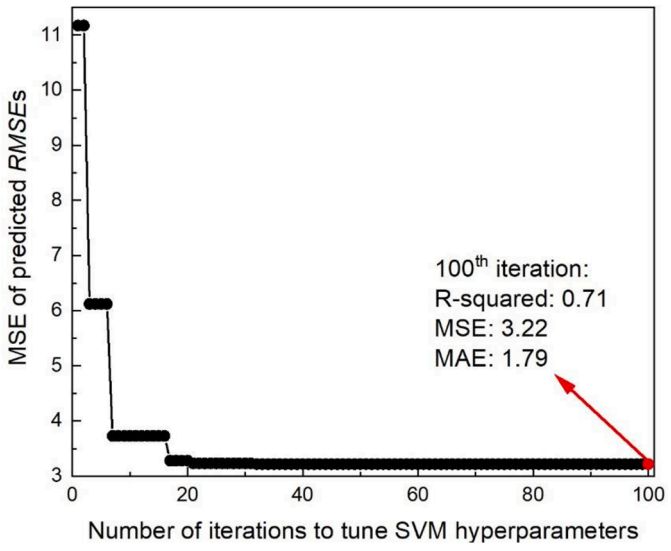

Fig. 7. Iterative hyperparameter tuning of the SVR model to minimize the MSE of predicted *RMSEs*.

The stress-strain responses of the CG and AA models are compared in Fig. 5. The elapsed (wall-clock) time associated with the CG simulation was less than an hour, down substantially from the almost 24 hours it took for the AA simulation to finish, showing a considerable efficiency achieved by coarse-graining. The softness and hardness of CG bead interactions depend on the value of individual CG-FF parameters and interplays thereof. Here, the reproduction of structural features of the AA model by the CG model was considered secondary in favor of simplicity and computational cost. Also, the literature suggests that CG-MD predictions can overestimate the mechanical properties of AA models (An et al., 2018; Duan et al., 2019; Shireen et al., 2022). Larger errors in the CG-MD results over AA-MD results in Fig. 5 are associated with uncertainty in averaging over 7,000 beads in the CG models compared with 42,000 atoms in the AA-MD model. Moreover, in MD simulations, high deformation rates (10^{-4} Å/fs) and fast ensemble sampling (time step of 0.5 fs) contribute to uncertainty propagation when the number of beads/atoms in a sample is relatively low.

The failure of the priors to fully capture the strain-stress response of the AA model could be attributed to the following reasons:

- Simplifications in CG models

One downside to converting AA models to CG models is losing intra-bead information. Each bond in the CG model of PVC, for instance, represented 11 bonds in the AA model. Although this simplification was the main impetus for creating CG models in the first place, the lost information associated with it introduced some errors into the CG model predictions.

- Chain length effect

The CG model parameters were quantified by studying the behavior of only 24 beads of a 1,000 bead model. In contrast, the comparison step involved simulating seven chains consisting of 1,000 beads (7,000 in total). This considerable increase in the number of chains influences the mechanical properties of polymers (Al-Nasassrah et al., 1998; Yazdani et al., 2019) because quantities derived from a small number of beads might not generalize to represent the mechanical properties of many chains with 1,000-bead for each.

- Insufficiency of harmonic expressions

Although the literature is rich in the use of CVFF to describe

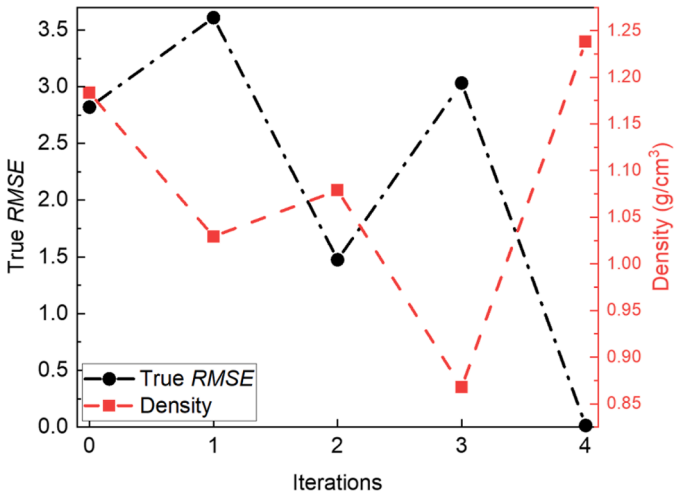

Fig. 8. Changes in *RMSE* and density of the 7,000-bead CG model resulting from SVR-assisted optimization of prior values.

interactions in the CG models of many types of polymers, the harmonic expressions inherent in CVFF fail to precisely capture all energy components among the beads, particularly under large deformations. Therefore, one source of uncertainty in the CG model would be the uncertainty in the implementation of CVFF to fully replicate the extracted properties of AA models.

- Uncertainties in priors

Another source of error in CG models could be the uncertainties associated with the priors. For example, as previously mentioned, the priors of the bond and angle equilibrium parameters (i.e. r_0 and θ_0) were the most frequent values over a long simulation time. These parameters, however, are not deterministic and subject to slight fluctuations or variations that can contribute to the departure of the CG response from the AA response.

3.2. SVR-assisted calibration of the priors

The performances of the surrogate models trained using the first generation of observations are shown in Fig. 6. R-squared values in the range 0.7–0.8 were achieved (Fig. 6), indicating an acceptable accuracy for the SVR models given the small size of the dataset. The history of hyperparameter tuning of the *RMSE* SVR model is shown in Fig. 7. Its mean squared error (MSE) sharply fell in the first 20 hyperparameter-tuning iterations. MSE, meant to punish significant errors in prediction, is one of the most common loss functions that is calculated by averaging the square of the difference between the model predictions and the ground truth across the entire dataset. Its closeness to the square of MAE (in other words, the proximity of MAE to RMSE) indicates the absence of significant errors in predictions.

Changes in the *RMSE* and density of the CG model due to the SVR-assisted, iterative calibration of the priors are shown in Fig. 8. Iteration 0 corresponds to the reference observation (i.e. priors). Results

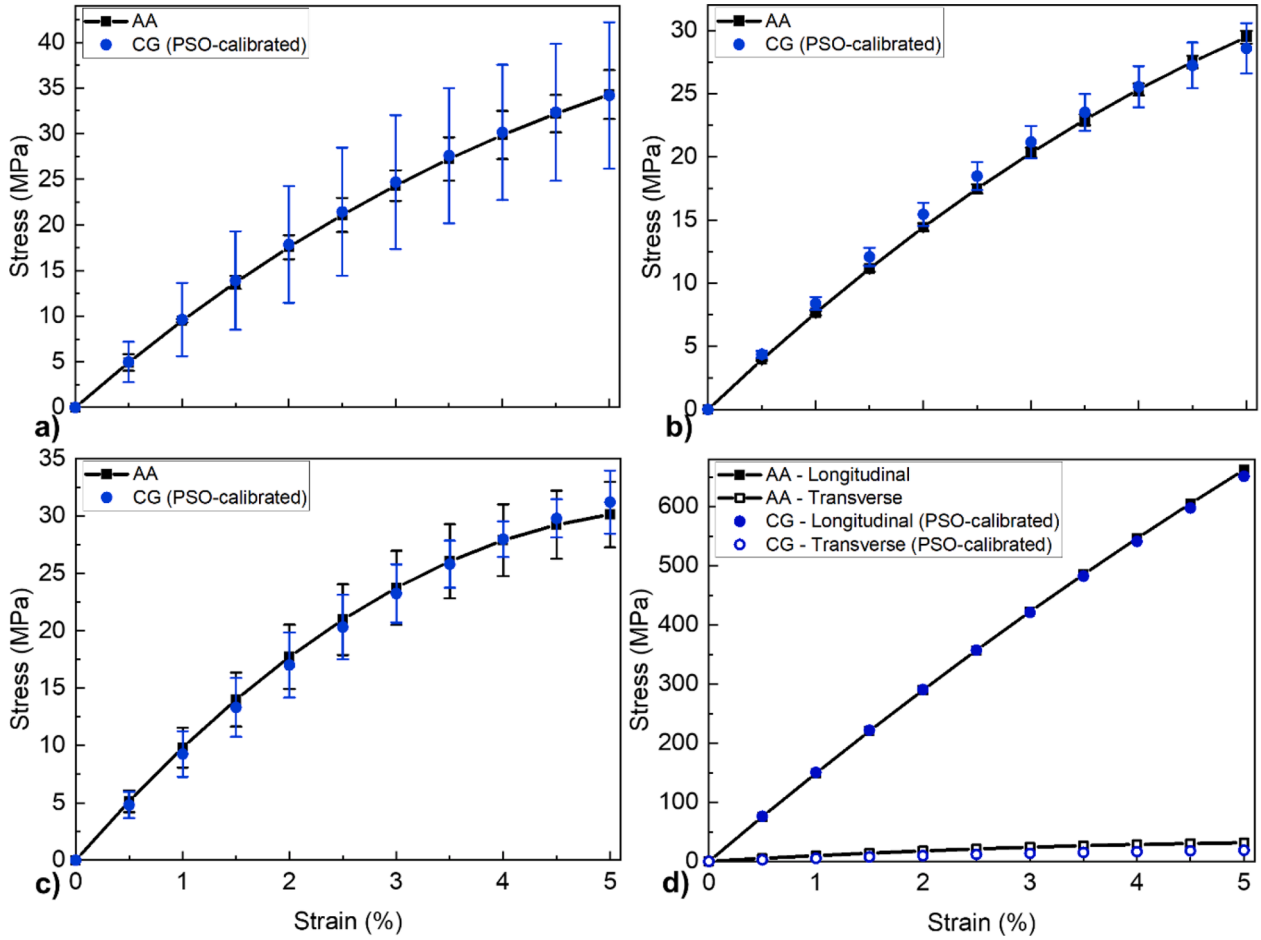

Fig. 9. Comparison of strain-stress response of AA model and that of PSO-calibrated CG models with a) 7,000 beads, b) 20,000 beads, and c) 40,000 beads; d) comparison of strain-stress responses in longitudinal and transverse directions of a CNT-reinforced PVC model. The error bars represent one standard deviation from the mean results of three simulations with different seed numbers. Error bars in (d) were small and removed for clarity.

Table 3
PSO-derived values for CG-FF parameters.

CG parameter	PSO-calibrated value	Change wrt prior (%)
r_0 (Å)	5.1	41.7
K_r (kcal/mol/Å^2)	12.5	–25.0
θ_0 (°)	171.3	34.8
K_θ (kcal/mol/rad^2)	4.9	–2.0
K_Φ (kcal/mol)	5.8	0.0
ε (kcal/mol)	1.1	–50.0
σ (Å)	3.6	–34.5

indicate that *RMSE* almost vanished, and density converged to its AA value of 1.22 g/cm^3 in only four iterations. Since *RMSE* did not decrease monotonically, it was not feasible to define a stopping criterion for the iterations, and the iterations were terminated when acceptable accuracies for the predicted density and stress-strain response at a given iteration were achieved.

Figs. 8a-c compare the stress-strain responses of the AA and PSO-calibrated CG models containing 7,000, 20,000, and 40,000 beads. Overall, the results show that the CG models well represented the AA model and captured its tensile response. The relatively larger error bars observed for the 7,000-bead CG model (Fig. 9a) can be attributed to the size effect. An exact match is also observed between the AA and CG models in composite form (Fig. 9d). The higher accuracy of the CNT-filled CG models compared with their pristine counterparts, especially in the CNT longitudinal direction, could be attributed to the substantially higher stiffness of the CNT that allows it to have a greater contribution to carrying the tensile load, leaving little to no meaningful contribution from the polymer matrix (Yazdani et al., 2017a, 2019). Another observation is that the error bars calculated across three replicates (different seed numbers) decreased as the model size increased from 7,000 to 20,000 and 40,000 beads (Fig. 9a vs. Fig. 9b and Fig. 9c).

The PSO-calibrated values of the CG-FF parameters are shown in Table 3. Five of the seven parameters had more than ±20% change from their priors. Such large deviations point to the inefficiency of traditional optimization methods, trial and error, and educated guesses at calibrating CG models.

As previously stated, T_g, thermal conductivity, and end-to-end distance of polymer chains were used to examine whether the optimized CG-FF would accurately predict the properties that it was not optimized against. Consistent with previous studies that showed the accuracy of CG models in predicting the T_g of AA models (Duan et al., 2019; Morita et al., 2006; Shireen et al., 2022; Yang et al., 2014), the results shown in Fig. 10 indicate a very close agreement between the T_g values obtained

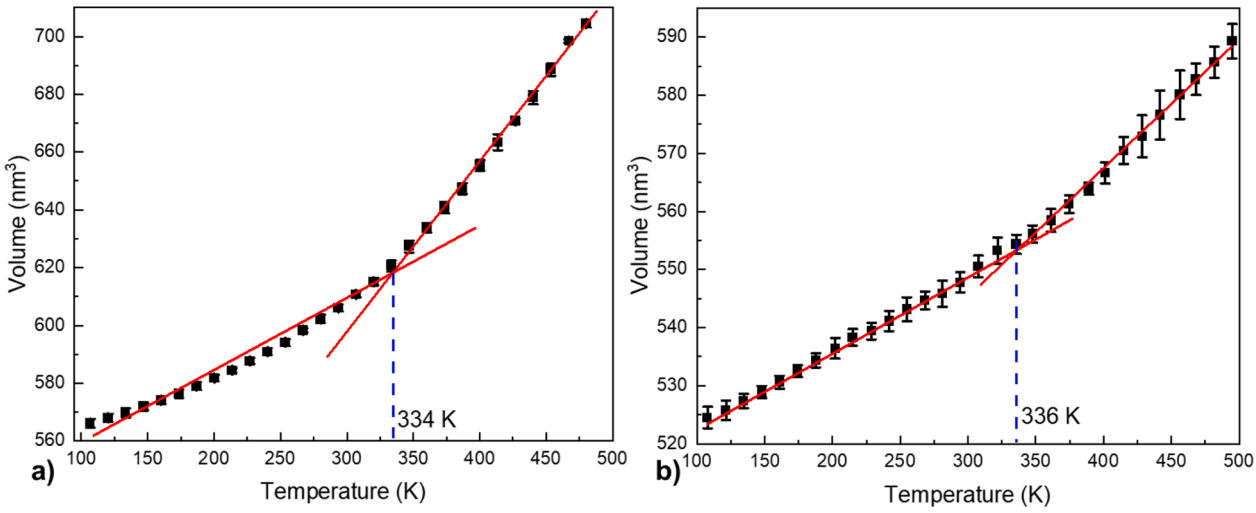

Fig. 10. Variation of volume by varying temperature from 500 K to 100 K with cooling rate of 1 K/ps for a) AA and b) CG models.

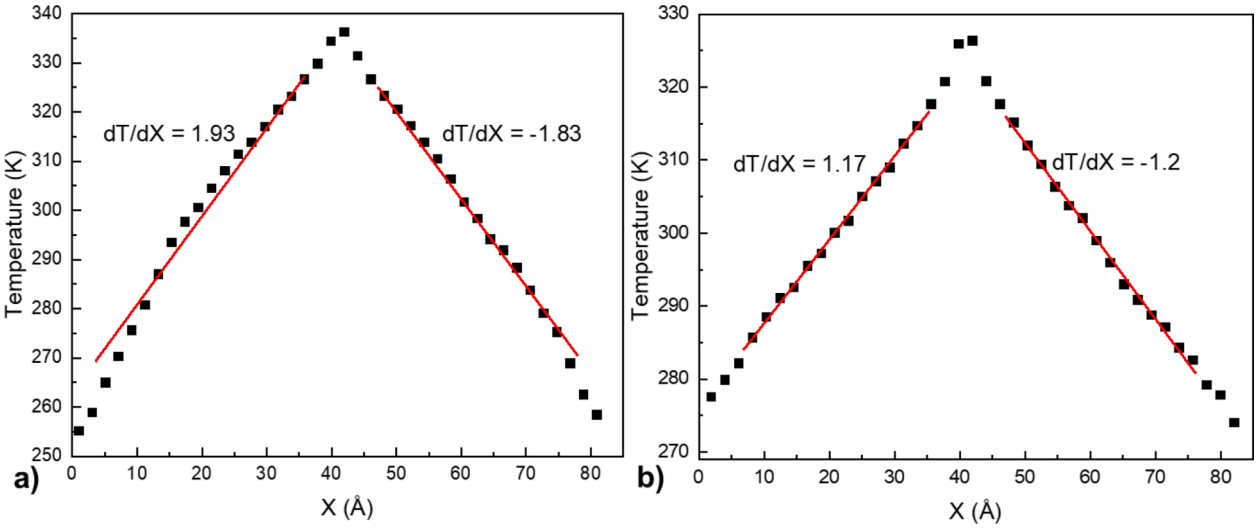

Fig. 11. Temperature profile created by swapping kinetic energy between low-/high-end slabs in RNEMD simulation of a) AA and b) CG models.

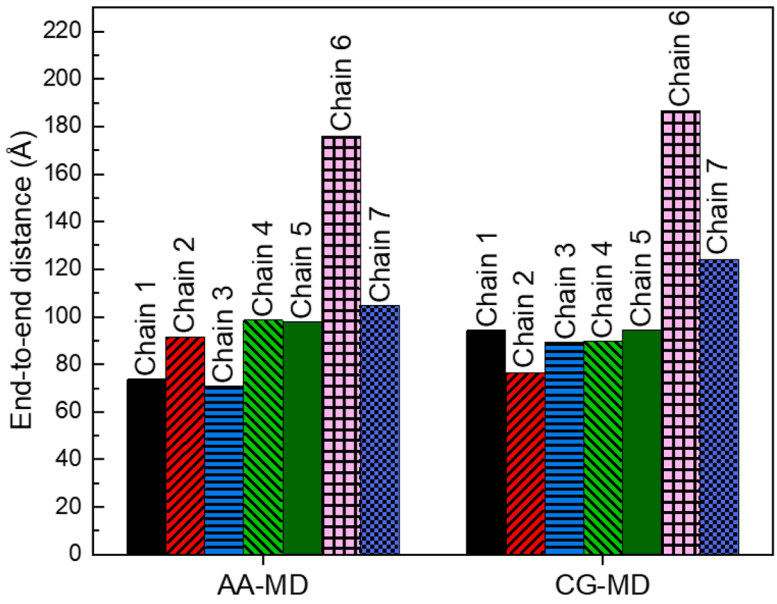

Fig. 12. The end-to-end distance comparison between AA-MD and CG-MD models of 7,000 monomers (seven 1,000-monomer chains).

using the AA and CG models (334 K vs. 336 K). The larger error bars of CG-MD models can be attributed to the smaller number of CG beads (7,000) than atoms in the AA model (42,000).

The thermal conductivity of amorphous polymers is typically very low and ranges from 0.1 W/m/K to 0.5 W/m/K for different types of bulk polymers (Sæther et al., 2021). In this study, based on the EMD approach, the thermal conductivity of the CG model was found to be 0.17 W/m/K, which is close to that of 0.25 W/m/K for the AA model.

The temperature profiles created by swapping the kinetic energy between the edge and middle slabs of PVC are shown in Fig. 11. The thermal conductivity of the AA and CG models using the RNEMD approach was calculated to be 0.11 and 0.22 W/m/K, respectively, which are close to the experimental values of 0.16–0.19 W/m/K (Han and Fina, 2011; Mamunya et al., 2002).

The end-to-end distances of seven chains with 1,000 monomers in CG-MD and AA-MD models are shown in Fig. 12. As it is seen, the end-to-end distances of both models are fairly similar, indicating that the CG-MD model can somewhat retain the structural features of the AA-MD model. However, even though the CG-MD model had a reasonably good prediction of the end-to-end distance of polymer chains, the observations for bond and angle distributions of monomers were not promising, suggesting that further attention should be given to replicating the structural features of the CG-MD model in future works.

4. Conclusion

A sustainable built environment is critical to propelling a country's economic growth. Polymers and polymer nanocomposites (PNCs) can be tuned to offer a lightweight, multifunctional, high-performance alternative to conventional construction materials and contribute to reducing the carbon footprint of the construction industry. Efforts, however, should be made to accelerate their transition from demonstration-scale to real-world applications by developing verified and validated computational paradigms, techniques, and models that can serve as a means to investigate the behavior of these materials in different circumstances.

Coarse graining is a promising approach to creating relatively larger yet representative models of materials for atomistic and molecular-scale simulations. Such simulations require coarse-grained (CG) force fields (CG-FFs) to describe interatomic or interparticle interactions among atoms and particles. Therefore, efforts should be made to reduce the otherwise high computational cost of developing CG-FFs. This study developed an approach to parameterize CG-FFs in an energy-conserving scheme. The approach involved coupling the particle swarm optimization (PSO) algorithm as the calibrator (optimizer) with two support vector regression (SVR)-based surrogate models (one for density and one for the stress-strain response) as the predictors. More specifically, it involved four stages: 1) simulating a reference all-atom (AA) model to find initial values (priors) for the CG-FF parameters, creating one "observation," 2) systematically perturbing the priors to create additional observations later AA-MD- and CG-MD-simulated to establish their stress-strain response, 3) training the two SVR models using the observations, and 4) iteratively calibrating the priors using SVR-assisted PSO and adding the newly calibrated priors to the SVR dataset to improve the accuracy of SVR predictions. The approach was demonstrated by developing a CG-FF for the mechanical properties and density of PVC. The CG-FF was also tested for reproducing some properties it was not optimized against (glass transition temperature, thermal conductivity, and end-to-end distance). Although the CG-FF was reasonably accurate in modeling these properties, further investigation is required to ascertain whether the underlying dynamics were captured and if the CG-FF can predict other thermal properties such as thermal expansion and heat capacity. Nevertheless, the presented approach is generic and can be used to formulate CG-FFs for simulating other polymers and PNCs toward shining light on mechanisms and phenomena governing their behavior. Such insight can help produce lighter polymers and PNCs with improved properties, in turn reducing embodied carbon and emissions, diverting as much waste from landfills as possible, and promoting sustainability in the built environment.

CRediT authorship contribution statement

Hamid Ghasemi: Investigation, Formal analysis, Visualization, Writing – original draft. **Hessam Yazdani:** Conceptualization, Resources, Writing – original draft, Writing – review & editing, Supervision, Project administration, Funding acquisition.

Declaration of Competing Interest

The authors do not have any competing interests to declare.

Data availability

The data supporting this study's findings are available from the corresponding author upon reasonable request.

Acknowledgments

This material is based upon work supported by the U.S. National Science Foundation under Grant CMMI 2046332. Some of the computing for this project was performed at the OU Supercomputing Center for Education & Research (OSCER) at the University of Oklahoma (OU).

References

Al-Nasassrah, M.A., Podczeck, F., Newton, J.M., 1998. The effect of an increase in chain length on the mechanical properties of polyethylene glycols. Eur. J. Pharm. Biopharm. Off. J. Arbeitsgemeinschaft Pharm. Verfahrenstechnik EV 46, 31–38. https://doi.org/10.1016/s0939-6411(97)00151-3.

An, Y., Bejagam, K.K., Deshmukh, S.A., 2018. Development of New Transferable Coarse-Grained Models of Hydrocarbons. J. Phys. Chem. B 122, 7143–7153. https://doi.org/10.1021/acs.jpcb.8b03822.

Arash, B., Park, H.S., Rabczuk, T., 2015. Mechanical properties of carbon nanotube reinforced polymer nanocomposites: A coarse-grained model. Compos. Part B Eng. 80, 92–100. https://doi.org/10.1016/j.compositesb.2015.05.038.

Bagri, A., Kim, S.-P., Ruoff, R.S., Shenoy, V.B., 2011. Thermal transport across Twin Grain Boundaries in Polycrystalline Graphene from Nonequilibrium Molecular Dynamics Simulations. Nano Lett 11, 3917–3921. https://doi.org/10.1021/nl202118d.

Chen, H., Qian, C., Liang, C., Kang, W., 2018. An approach for predicting the compressive strength of cement-based materials exposed to sulfate attack. PLoS ONE 13. https://doi.org/10.1371/journal.pone.0191370.

Christensen, R., Sørensen, S.S., Liu, H., Li, K., Bauchy, M., Smedskjaer, M.M., 2021. Interatomic potential parameterization using particle swarm optimization: Case study of glassy silica. J. Chem. Phys. 154, 134505 https://doi.org/10.1063/5.0041183.

Cui, J.-Y., Cai, Y.-B., Yuan, W.-J., Lv, Z.-F., Zhang, C., Xu, S.-A., 2017. Preparation of PMMA grafted calcium carbonate whiskers and its reinforcement effect in PVC. Polym. Compos. 38, 2753–2761. https://doi.org/10.1002/pc.23873.

Duan, K., He, Y., Li, Y., Liu, J., Zhang, J., Hu, Y., Lin, R., Wang, X., Deng, W., Li, L., 2019. Machine-learning assisted coarse-grained model for epoxies over wide ranges of temperatures and cross-linking degrees. Mater. Des. 183, 108130 https://doi.org/10.1016/j.matdes.2019.108130.

Eslami, H., Khani, M., Müller-Plathe, F., 2019. Gaussian Charge Distributions for Incorporation of Electrostatic Interactions in Dissipative Particle Dynamics: Application to Self-Assembly of Surfactants. J. Chem. Theory Comput. 15, 4197–4207. https://doi.org/10.1021/acs.jctc.9b00174.

Eslami, H., Mohammadzadeh, L., Mehdipour, N., 2011. Reverse nonequilibrium molecular dynamics simulation of thermal conductivity in nanoconfined polyamide-6,6. J. Chem. Phys. 135, 064703 https://doi.org/10.1063/1.3623471.

Eslami, H., Müller-Plathe, F., 2013. Coarse-Grained Molecular Dynamics Simulations of Polyamide-6,6 on Graphene. J. Phys. Chem. C 117, 5249–5257. https://doi.org/10.1021/jp400142h.

Español, P., Serrano, M., Pagonabarraga, I., Zúñiga, I., 2016. Energy-conserving coarse-graining of complex molecules. Soft Matter 12, 4821–4837. https://doi.org/10.1039/C5SM03038B.

Fini, E.H., Poulikakos, L., Christiansen, J., de, C., Schmidt, W., Parast, M.M., 2021. Toward sustainability in the built environment: An integrative approach. Resour. Conserv. Recycl. 172 https://doi.org/10.1016/j.resconrec.2021.105676.

Gharehbaghi, S., Yazdani, H., Khatibinia, M., 2019. Estimating inelastic seismic response of reinforced concrete frame structures using a wavelet support vector machine and an artificial neural network. Neural Comput. Appl. 32, 2975–2988. https://doi.org/10.1007/s00521-019-04075-2.

Hagler, A.T., Lifson, S., Dauber, P., 1979. Consistent force field studies of intermolecular forces in hydrogen-bonded crystals. 2. A benchmark for the objective comparison of alternative force fields. J. Am. Chem. Soc. 101, 5122–5130. https://doi.org/10.1021/ja00512a002.

Han, Z., Fina, A., 2011. Thermal conductivity of carbon nanotubes and their polymer nanocomposites: A review. Prog. Polym. Sci., Special Issue on Composites 36, 914–944. https://doi.org/10.1016/j.progpolymsci.2010.11.004.

Hossain, D., Tschopp, M.A., Ward, D.K., Bouvard, J.L., Wang, P., Horstemeyer, M.F., 2010. Molecular dynamics simulations of deformation mechanisms of amorphous polyethylene. Polymer 51, 6071–6083. https://doi.org/10.1016/j.polymer.2010.10.009.

Jain, S., Garde, S., Kumar, S.K., 2006. Do Inverse Monte Carlo Algorithms Yield Thermodynamically Consistent Interaction Potentials? Ind. Eng. Chem. Res. 45, 5614–5618. https://doi.org/10.1021/ie060042h.

Kazemi, M., Faisal Kabir, S., Fini, E.H., 2021. State of the art in recycling waste thermoplastics and thermosets and their applications in construction. Resour. Conserv. Recycl. 174, 105776 https://doi.org/10.1016/j.resconrec.2021.105776.

Kazemi, M., Fini, E.H., 2022. State of the art in the application of functionalized waste polymers in the built environment. Resour. Conserv. Recycl. 177, 105967 https://doi.org/10.1016/j.resconrec.2021.105967.

Kennedy, J., Eberhart, R., 1995. Particle swarm optimization. In: Proceedings of IEEE International Conference on Neural Networks. Perth, Australia, pp. 1942–1948.

Khatibinia, M., Yazdani, H., 2018. Accelerated multi-gravitational search algorithm for size optimization of truss structures. Swarm Evol. Comput. 38, 109–119. https://doi.org/10.1016/j.swevo.2017.07.001.

Kubo, R., 1957. Statistical-Mechanical Theory of Irreversible Processes. I. General Theory and Simple Applications to Magnetic and Conduction Problems. J. Phys. Soc. Jpn. 12, 570–586. https://doi.org/10.1143/JPSJ.12.570.

Lampin, E., Palla, P.L., Francioso, P.-A., Cleri, F., 2013. Thermal conductivity from approach-to-equilibrium molecular dynamics. J. Appl. Phys. 114, 033525 https://doi.org/10.1063/1.4815945.

Lange, J., Souza, F.G.de, Nele, M., Tavares, F.W., Segtovich, I.S.V., Silva, G.C.Q.da, Pinto, J.C., 2016. Molecular Dynamic Simulation of Oxaliplatin Diffusion in Poly (lactic acid-co-glycolic acid). Part A: Parameterization and Validation of the Force-Field CVFF. Macromol. Theory Simul. 25, 45–62. https://doi.org/10.1002/mats.201500049.

Liwo, A., Czaplewski, C., 2020. Extension of the force-matching method to coarse-grained models with axially symmetric sites to produce transferable force fields: Application to the UNRES model of proteins. J. Chem. Phys. 152, 054902 https://doi.org/10.1063/1.5138991.

Lu, W.-C., Ji, X.-B., Li, M.-J., Liu, L., Yue, B.-H., Zhang, L.-M., 2013. Using support vector machine for materials design. Adv. Manuf. 1, 151–159. https://doi.org/10.1007/s40436-013-0025-2.

Lussetti, E., Terao, T., Müller-Plathe, F., 2007. Nonequilibrium Molecular Dynamics Calculation of the Thermal Conductivity of Amorphous Polyamide-6,6. J. Phys. Chem. B 111, 11516–11523. https://doi.org/10.1021/jp0737956.

Mamunya, Ye.P., Davydenko, V.V., Pissis, P., Lebedev, E.V., 2002. Electrical and thermal conductivity of polymers filled with metal powders. Eur. Polym. J. 38, 1887–1897. https://doi.org/10.1016/S0014-3057(02)00064-2.

Mannodi-Kanakkithodi, A., Pilania, G., Ramprasad, R., 2016. Critical assessment of regression-based machine learning methods for polymer dielectrics. Comput. Mater. Sci. 125, 123–135. https://doi.org/10.1016/j.commatsci.2016.08.039.

Marrink, S.J., Risselada, H.J., Yefimov, S., Tieleman, D.P., de Vries, A.H., 2007. The MARTINI Force Field: Coarse Grained Model for Biomolecular Simulations. J. Phys. Chem. B 111, 7812–7824. https://doi.org/10.1021/jp071097f.

Morita, H., Tanaka, K., Kajiyama, T., Nishi, T., Doi, M., 2006. Study of the Glass Transition Temperature of Polymer Surface by Coarse-Grained Molecular Dynamics Simulation. Macromolecules 39, 6233–6237. https://doi.org/10.1021/ma052632h.

Mozer, M.C., Jordan, M.I., Petsche, T., 1997. Advances in Neural Information Processing Systems. In: Proceedings of the 1996 Conference, 9. MIT Press.

Müller-Plathe, F., 2002. Coarse-Graining in Polymer Simulation: From the Atomistic to the Mesoscopic Scale and Back. ChemPhysChem 3, 754–769. https://doi.org/10.1002/1439-7641(20020916)3:9<754::AID-CPHC754>3.0.CO;2-U.

Müller-Plathe, F., 1997. A simple nonequilibrium molecular dynamics method for calculating the thermal conductivity. J. Chem. Phys. 106, 6082–6085. https://doi.org/10.1063/1.473271.

Müller-Plathe, F., Bordat, P., 2004. Reverse Non-equilibrium Molecular Dynamics. In: Karttunen, M., Lukkarinen, A., Vattulainen, I. (Eds.), Novel Methods in Soft Matter Simulations, Lecture Notes in Physics. Springer, Berlin, Heidelberg, pp. 310–326. https://doi.org/10.1007/978-3-540-39895-0_10.

Oden, J.T., Farrell, K., Faghihi, D., 2015. Estimation of error in observables of coarse-grained models of atomic systems. Adv. Model. Simul. Eng. Sci. 2, 5. https://doi.org/10.1186/s40323-015-0025-9.

Oden, J.T., Prudencio, E.E., Bauman, P.T., 2013. Virtual model validation of complex multiscale systems: Applications to nonlinear elastostatics. Comput. Methods Appl. Mech. Eng. 266, 162–184. https://doi.org/10.1016/j.cma.2013.07.011.

Plimpton, S., 1995. Fast Parallel Algorithms for Short-Range Molecular Dynamics. J. Comput. Phys. 117, 1–19. https://doi.org/10.1006/jcph.1995.1039.

Puppala, A.J., Banerjee, A., Congress, S.S.C., 2020. 7 - Geosynthetics in geo-infrastructure applications. In: Reifsnider, K.L. (Ed.), Durability of Composite Systems, Woodhead Publishing Series in Composites Science and Engineering. Woodhead Publishing, pp. 289–312. https://doi.org/10.1016/B978-0-12-818260-4.00007-7.

Razzaghi, L., Khalkhali, M., Rajabpour, A., Khoeini, F., 2021. Effect of graphene and carbon-nitride nanofillers on the thermal transport properties of polymer nanocomposites: A combined molecular dynamics and finite element study. Phys. Rev. E 103, 013310. https://doi.org/10.1103/PhysRevE.103.013310.

Rudzinski, J.F., Noid, W.G., 2015. Bottom-Up Coarse-Graining of Peptide Ensembles and Helix–Coil Transitions. J. Chem. Theory Comput. 11, 1278–1291. https://doi.org/10.1021/ct5009922.

Sæther, S., Falck, M., Zhang, Z., Lervik, A., He, J., 2021. Thermal Transport in Polyethylene: The Effect of Force Fields and Crystallinity. Macromolecules 54, 6563–6574. https://doi.org/10.1021/acs.macromol.1c00633.

Shayesteh Bilondi, M.R., Yazdani, H., Khatibinia, M., 2018. Seismic energy dissipation-based optimum design of tuned mass dampers. Struct. Multidiscip. Optim. 58, 2517–2531. https://doi.org/10.1007/s00158-018-2033-0.

Shi, Y., Eberhart, R., 1998. A modified particle swarm optimizer. In: 1998 IEEE International Conference on Evolutionary Computation Proceedings. IEEE World Congress on Computational Intelligence (Cat. No.98TH8360). Presented at the 1998 IEEE International Conference on Evolutionary Computation Proceedings. IEEE World Congress on Computational Intelligence (Cat. No.98TH8360), pp. 69–73. https://doi.org/10.1109/ICEC.1998.699146.

Shireen, Z., Weeratunge, H., Menzel, A., Phillips, A.W., Larson, R.G., Smith-Miles, K., Hajizadeh, E., 2022. A novel machine learning enabled hybrid optimization framework for efficient and transferable coarse-graining of a model polymer. ArXiv220413295. Phys.

Shukla, S.K., 2021. Geosynthetics and Ground Engineering: Sustainability Considerations. Int. J. Geosynth. Ground Eng. 7, 17. https://doi.org/10.1007/s40891-021-00256-z.

Smola, A.J., Schölkopf, B., 2004. A tutorial on support vector regression. Stat. Comput. 14, 199–222. https://doi.org/10.1023/B:STCO.0000035301.49549.88.

Stukowski, A., 2009. Visualization and analysis of atomistic simulation data with OVITO–the Open Visualization Tool. Model. Simul. Mater. Sci. Eng. 18, 015012 https://doi.org/10.1088/0965-0393/18/1/015012.

Sun, T., Minhas, V., Korolev, N., Mirzoev, A., Lyubartsev, A.P., Nordenskiöld, L., 2021. Bottom-Up Coarse-Grained Modeling of. DNA. Front. Mol. Biosci. 8.

Vapnik, V., 2000. The Nature of Statistical Learning Theory. Information Science and Statistics, 2nd ed. Springer-Verlag, New York. https://doi.org/10.1007/978-1-4757-3264-1.

Vasilev, A., Lorenz, T., Breitkopf, C., 2020. Thermal Conductivity of Polyisoprene and Polybutadiene from Molecular Dynamics Simulations and Transient Measurements. Polymers 12, 1081. https://doi.org/10.3390/polym12051081.

Yang, S., Cui, Z., Qu, J., 2014. A Coarse-Grained Model for Epoxy Molding Compound. J. Phys. Chem. B 118, 1660–1669. https://doi.org/10.1021/jp409297t.

Yazdani, H., Ghasemi, H., Wallace, C., Hatami, K., 2019. Mechanical properties of carbon nanotube-filled polyethylene composites: a molecular dynamics simulation study. Polym. Compos.

Yazdani, H., Hatami, K., Eftekhari, M., 2017a. Mechanical properties of single-walled carbon nanotubes: a comprehensive molecular dynamics study. Mater. Res. Express 4, 055015. https://doi.org/10.1088/2053-1591/aa7003.

Yazdani, H., Khatibinia, M., Gharehbaghi, S., Hatami, K., 2017b. Probabilistic Performance-Based Optimum Seismic Design of RC Structures Considering Soil–Structure Interaction Effects. ASCE-ASME J. Risk Uncertain. Eng. Syst. Part Civ. Eng. G4016004. https://doi.org/10.1061/AJRUA6.0000880.

Zakertabrizi, M., Hosseini, E., Sukumaran, S., Korayem, A.H., Fini, E.H., 2021. Turning two waste streams into one solution for enhancing sustainability of the built environment. Resour. Conserv. Recycl. 174, 105778 https://doi.org/10.1016/j.resconrec.2021.105778.